The velocity field around a Taylor bubble rising in a stagnant viscous fluid: numerical and experimental results

J.D. Bugg [*], G.A. Saad

Department of Mechanical Engineering, University of Saskatchewan, 57 Campus Drive, Saskatoon, Saskatchewan, Canada S7N 5A9

Abstract

Particle image velocimetry (PIV) measurements have been made around a rising Taylor bubble. The bubble was produced by injecting air into a tube containing stagnant olive oil. The fluid properties and tube diameter yielded Eötvös = 100, Morton = 0.015, and Reynolds = 27. Measurements were made in the region ahead of the bubble, in the falling film, and in the wake. The PIV system used pulsed Nd:YAG lasers and a digital cross-correlation camera. The measurements achieved a spatial resolution of 0.0079 tube diameters. Verification of the results was illustrated by a mass flow balance in the falling film.

The flow was also predicted using a volume-of-fluid based finite difference technique and the results compared to the PIV measurements. The comparison was very good over most of the flow and confirms the validity of the numerical model. © 2002 Elsevier Science Ltd. All rights reserved.

Keywords: Particle image velocimetry; Two-phase flow; Taylor bubbles; Wakes; Computational fluid dynamics; Moving interface methods

1. Introduction

In this work, the problem of a large bubble rising through a circular tube containing a stagnant fluid is addressed. Because the bubble is large, it takes on an elongated shape and is often referred to as a Taylor bubble. The general shape of a Taylor bubble is a bubble whose length is several times the tube diameter and whose leading edge is rounded. The trailing edge can take on either a rounded, indented, or unsteady shape depending upon the flow conditions and fluid properties. This flow is of fundamental importance in gas–liquid two-phase flows in circular ducts and is

---

[*] Corresponding author. Tel.: +1-306-966-5469; fax: +1-306-966-5427.

E-mail address: jim.bugg@usask.ca (J.D. Bugg).

particularly relevant to the slug flow regime which occurs at intermediate void fractions with relatively low liquid flow rates. Slug flow occurs widely in hydrocarbon production and transportation, chemical and nuclear reactors, and heat transport systems where phase change takes place. The differences between this study and the more general case of slug flow are that the superficial liquid velocity is zero (stagnant fluid) and the study only considers a single bubble. However, the fundamental importance of the Taylor bubble in slug flow make it a case that is often modelled in an effort to develop or validate numerical models for two-phase flow.

Both numerical and experimental results for a Taylor bubble rising in a vertical tube were obtained and the ability of the numerical model to predict the velocity field will be discussed in this paper. This discussion will take place based on the velocity field around the bubble.

White and Beardmore (1962) describe a wide range of experimental results on Taylor bubbles rising through stagnant liquids in vertical tubes. However, because of the instruments available, the information is restricted to terminal velocities. They identify Eötvös number ($Eo = \rho g D^2/\sigma$) and Morton number ($Mo = g\eta^4/(\rho\sigma^3)$) as useful parameters with which to predict the rise velocity of the bubbles. The rise velocity was presented in non-dimensional form as a Froude number ($Fr = U_t/\sqrt{gD}$). In these groups U_t is the terminal speed, g is the acceleration due to gravity, D is the tube diameter, ρ is the liquid density, σ is the surface tension, and η is the dynamic viscosity of the liquid. Others have also used the Reynolds number and the Weber number as parameters. By including the data of several other workers, White and Beardmore (1962) produced a comprehensive graphical correlation of Froude number as a function of Eötvös number and Morton number. They also discussed the relative importance of viscous forces, interfacial effects, and inertial effects in different regions of this map. For the particular conditions investigated experimentally in the present work, the map of White and Beardmore (1962) indicates that interfacial forces are unimportant.

Fabre and Liné (1992) reviewed the motion of Taylor bubbles as part of a larger review of slug flow. They specifically considered the case of zero liquid flow in vertical tubes as is being studied in this paper. They stated that Taylor bubbles were characterised by leading edges shaped like prolate spheroids followed by a film on the wall of the tube and finally a trailing edge. This trailing edge would be flat in cases were viscosity is unimportant and would be an oblate spheroid in cases where viscosity is important. The groups they used to characterise slug flow are the Eötvös number and a "dimensionless inverse viscosity", $N_f = (Eo^3/Mo)^{1/4} = \sqrt{\rho^2 g D^3/\eta^2}$. They state that the viscous regime is encountered for $N_f < 2$. In the measurements presented in this paper, $N_f = 90$ indicating that both viscous and inertial effects are important. This is consistent with the classification of White and Beardmore (1962).

Mao and Dukler (1990, 1991) developed a numerical model of the flow around a Taylor bubble using a curvilinear coordinate system attached to the bubble and fitted to the bubble shape. The technique adjusted the shape of the interface so that the normal stress at the interface satisfied the condition of constant pressure inside the bubble. The terminal velocity of the bubble, and therefore the reference frame velocity, was adjusted until the bubble was locally spherical at the nose. The solution domain extended only to the trailing edge of the bubble and not into the wake region.

The goal of the experiments was to produce high-resolution particle image velocimetry (PIV) measurements. PIV holds tremendous potential as a tool for validating computational fluid dynamics predictions and for understanding fluid flow from a purely experimental perspective. Polonsky et al. (1999) studied the velocity field ahead of a Taylor bubble using interlaced video to

perform PIV. Because of limitations imposed on the minimum time between frames, they were not able to perform PIV in the film or wake region. The tube diameter (25 mm) and fluid properties (air–water) used by Polonsky et al. (1999) resulted in operation in the inertial regime where $Fr = 0.351$.

DeJesus et al. (1995) made detailed velocity field measurements around a Taylor bubble rising in a vertical tube using photochromic dye activation and image analysis. Velocity vectors were presented for the region near the bubble nose, in the falling film, and in the wake. The conditions reported correspond to $Eo = 194$ and $Mo = 2.9 \times 10^{-9}$. These conditions are such that inertia dominates viscous forces and a turbulent wake exists below the bubble. As a result, it is difficult to make meaningful comparisons of a single velocity field measurement in the wake region to the results of the numerical model used in this paper.

2. Numerical model

The numerical results to be presented here have been previously reported in Bugg et al. (1998). In that paper, simulations were reported over a wide range of Eötvös and Morton numbers. However, detailed velocity field information was only given for the case of $Eo = 100$ and $Mo = 10^{-12}$. For the conditions of interest in the present paper, only the bubble shape was reported. In this paper the details of the velocity field prediction will be compared to the PIV measurements.

The details of the numerical model were described in Bugg et al. (1998) and will be summarised here. The technique solved the transient governing equations in cylindrical coordinates using a standard pressure correction technique to handle the coupling between the velocity field and the pressure field. The convective and diffusive terms were treated explicitly. The diffusive terms were always central differenced and a type of hybrid differencing was used for the convective terms. The shape of the gas–liquid interface was predicted by the algorithm as part of the solution procedure. A volume-of-fluid specification was used to record the relative amounts of gas and liquid in each control volume. The donor–acceptor method (Hirt and Nichols, 1981) was used to calculate the fluxes of fluids between adjacent control volumes. Although it is recognised that this is a rather old technique, the results that will be presented show that it works well under these conditions. Note that no turbulence model was employed in these simulations.

The grid used to generate the numerical results was uniform and contained 25×400 control volumes in the radial and axial directions, respectively. The algorithm was initialised with an arbitrarily shaped bubble and allowed to run until a steady bubble shape was obtained. The final bubble shape obtained was independent of the initial bubble shape chosen. In the original paper (Bugg et al., 1998) the results were shown to be grid independent by repeating the simulation on a finer grid.

3. Experiments

The experiments reported here were also described in Saad and Bugg (2001). The Taylor bubbles were produced at the bottom of a vertical tube 19 mm in diameter. A schematic diagram
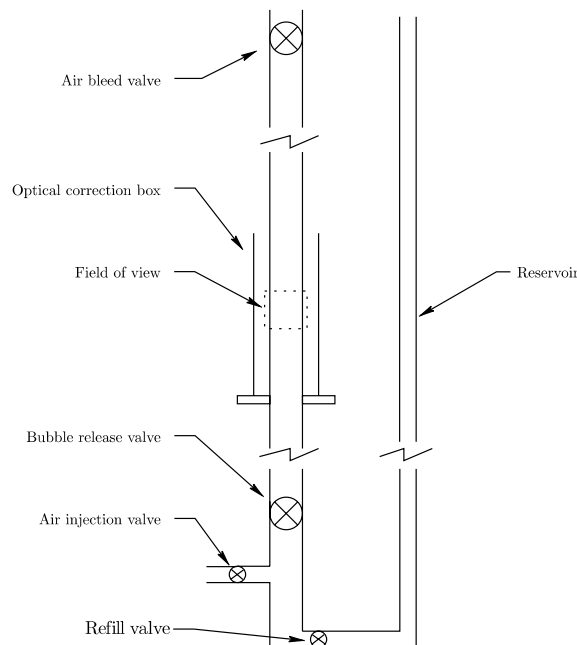
Fig. 1. Schematic of the vertical test section used to produce single Taylor bubbles rising in a stagnant fluid.

of the apparatus is shown in Fig. 1. A ball valve with a bore as close as possible to the tube's inner diameter was placed near the bottom of the tube (bubble release valve). Beginning with this valve closed, a carefully metered volume of air (10 cm³ at atmospheric pressure) was injected below the ball valve. This was done with the refill valve open so that the displaced fluid would move into the reservoir. After injection, the trapped volume of air below the bubble release valve was 15.5 cm³ which yielded a bubble length of approximately 10 cm. The chamber below the valve was then closed completely. In addition, the tube above the ball valve was closed at the top and completely full of liquid. This produced a closed tube so that the bubble would not grow as it rose. The ball valve was then opened to release the bubble. It was found that bubbles released in this manner behaved very consistently and rarely were small bubbles trapped in the wake of the large bubble. This was essential to obtain PIV measurements in the wake. After the bubble had reached the top of the tube, a vent was opened to bleed the air out before the next bubble was released. The field of view was 74 tube diameters from the bubble release valve.

The working fluid was olive oil. The density of the olive oil was measured by weighing a know volume and was found to be 911 kg/m³. The viscosity was measured at room temperature (19 °C) and was found to be 84 cP. The surface tension was measured with a rod tensiometer (Temco EZT-100) and found to be 0.0328 N/m. These fluid properties and tube diameter yield the following dimensionless numbers: $Eo = 100$, $Mo = 0.015$, and $Re = 27$.

The vertical tube was equipped with two phase detectors (not shown in Fig. 1) to detect the passage of the bubble. Each consisted of an infrared diode and detector. The beam from the diode traversed the tube diameter. The detector produced a pulse when the bubble interrupted the light from the diode. The phase detectors had two purposes; to measure the terminal velocity of the bubble and to trigger the PIV system.

The PIV system consisted of dual Nd:YAG lasers each with a nominal pulse energy of 50 mJ. A 6.4 mm focal length cylindrical lens and a 250 mm spherical lens gave a light sheet which covered the field-of-view adequately and had a thickness of approximately 60 μm at the tube axis. The illuminated plane was recorded with a Kodak MegaPlus ES1.0 camera with 1008×1018 active pixels. The camera was fitted with a 200 mm Micro-Nikkor AF, F-mount lens and an extension ring to allow close focusing. The vertical tube was enclosed in a square optical correction box and the region between the box and the tube was filled with olive oil. Olive oil has an index of refraction very close to glass. To confirm that image distortion was minimal in this configuration, a steel ruler with 0.254 mm (1/100 in.) divisions was placed in the measurement plane. An image was taken with the same lens system as the PIV measurements but using photographic film. This image was scanned (147 pixels/mm) and the ruler markings digitised. This procedure confirmed that the image calibration was constant all the way from the tube wall to the tube centreline.

The laser pulses and image acquisition had to be synchronised with the bubble position. Because very consistent bubble sizes could be generated and the rise velocity was very repeatable, the delay required between when the leading edge of the bubble triggered the lower phase detector and when it would be in the proper position for measurements was very repeatable. By adjusting the position of this phase detector, the position of the bubble in the field-of-view bubble could be selected. The laser pulse separation was controlled by a Berkeley Nucleonics 500B digital delay generator and was set to 1 ms for the results in this paper.

The seed particles were silicon carbide with a mean diameter of 2 μm and a specific gravity of 3.2. Proper seeding density was critical to the measurements. A seeding density of 2.5×10^{-6} gm/cm^3 was found to give sufficient particle image density to yield successful correlation.

The PIV system described above allowed interrogation areas of 0.304 mm $\times$ 0.304 mm corresponding to 16×16 pixels in the digitised image. This resolution was achieved by a three-pass analysis technique where the image is first analysed using 64×64 and then 32×32 pixel interrogation areas. At each stage, the displacement results from the previous stage are used to guide the offset of the interrogation windows in the next stage. Using this technique, it is possible to achieve rather high resolution even in regions where the particle displacement is larger than could normally be measured. The interrogation areas overlapped by 50% to nominally yield 125×126 velocity measurements and achieve a spatial resolution of 0.152 mm. A few of these measurements were not valid because the tube wall occupied a portion of the field-of-view. Sub-pixel resolution was achieved by local parabolic fits on the correlation plane. The correlation coefficient over most of reported field was in the range 0.7–0.8. The signal-to-noise ratio, defined here as the height of the signal peak divided by height of the highest noise peak on the correlation plane, ranged from about 2.5 to 3.0. Post-processing of the velocity field was done with a local 3×3 median filter.

Validation of the present measurements was performed by checking the mass balance calculated using the measurements. Consider the control volume shown in Fig. 2 which is moving upwards at the same velocity as the bubble. The flow is steady in this frame of reference and conservation of mass demands that, regardless of where the bottom surface of the control volume is located,

$$U_t \pi R^2 = 2\pi \int_{r_i}^{R} (U_t + v_z) r \, \mathrm{d}r$$
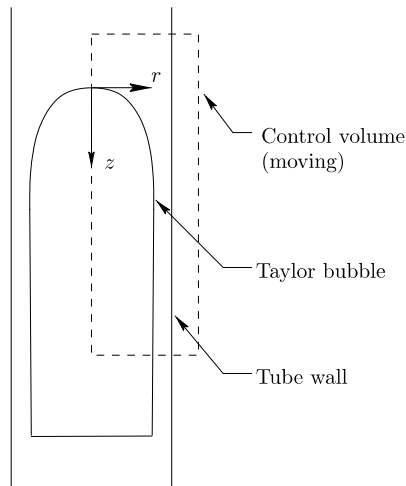
Fig. 2. The control volume used to validate the velocity measurements using a mass balance.

where U_t is the terminal velocity of the bubble, R is the tube radius, r_i is the radial coordinate of the gas–liquid interface, and v_z is the axial component of velocity measured in a stationary frame of reference. This equation can be rearranged to calculate the terminal velocity of the bubble based on the velocity profile measurements made at any axial location.

$$U_t = \frac{2}{r_i^2} \int_{r_i}^{R} v_z r \, dr$$

This integral was evaluated for several axial locations using the measured axial component of velocity and the resulting terminal velocity was within 3% of the terminal velocity measured using the phase transition detectors.

4. Results

The terminal velocity in the experiments was measured by time-of-flight between the two phase detectors. The phase detectors were placed 97.5 cm apart. The time for the bubble to travel between the two detectors was measured with a digital oscilloscope. The terminal velocity of the bubbles was measured to be 131 mm/s. This agrees with the theoretical value predicted by Brown (1965) and yields a Froude number of 0.303. This is within 7% of the value predicted by the numerical model (0.323).

The velocity field measurement obtained near the leading edge of the bubble is shown in Fig. 3. The velocity at the tip of the bubble essentially matches the bubble velocity (131 mm/s). Also, as demanded by the symmetry of the flow, there is no noticeable radial velocity along the tube axis ahead of the bubble. The axial component of velocity drops off quite rapidly ahead of the bubble. Fig. 4 compares the measured and predicted axial component of velocity on the tube axis as a function of the distance ahead of the bubble. At about $D/3$ ahead of the bubble, the velocity has reduced to about 5% of the bubble velocity.
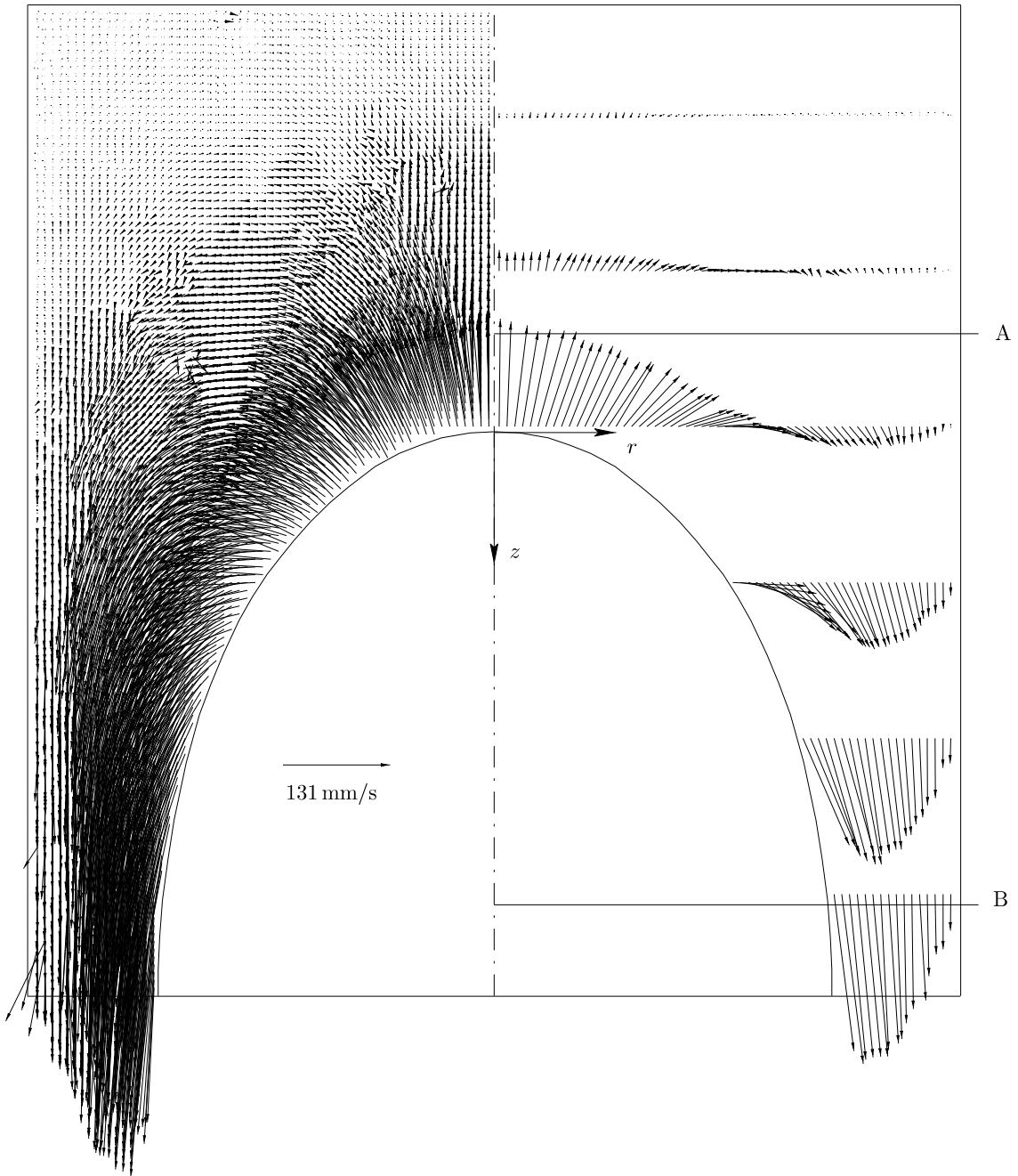
Fig. 3. PIV measurements of the velocity field measured near the leading edge of a Taylor bubble rising in a stagnant fluid. The left side of the axis of symmetry shows all the measurements while the right side shows only every twentieth axial location for clarity. The tube diameter is 19 mm.
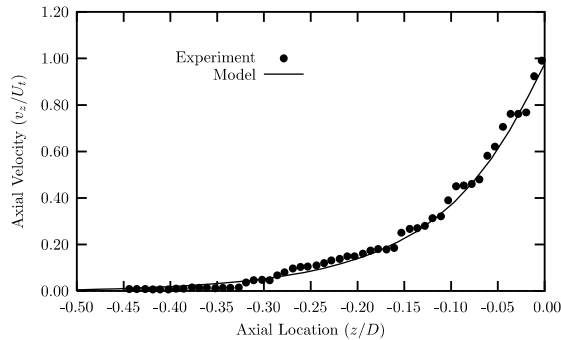
Fig. 4. The axial component of velocity along the tube axis above the bubble. The PIV measurements are compared to the numerical results.

The velocity field in the region near the top of the bubble but away from the tube axis is characterised by a strong radial velocity component. This is required to move the liquid into the falling film and allow passage of the bubble. This can be seen qualitatively in the vector plots of Fig. 3. A detailed quantitative comparison of the measurements and the model predictions is given in Fig. 5 for an axial location just above the bubble. This axial location is indicated in Fig. 3 as location A. The agreement in this region is excellent. There is some scatter apparent in the experimental results presented, however, these experimental results are essentially unfiltered. Although a 3×3 median filter was applied to the vector field, this only influenced a very small number of the measurements. This scatter is also apparent upon close inspection of the vector plots in Fig. 3 but becomes more pronounced when the individual velocity components are plotted. It should be noted that the experimental results presented are not ensemble averaged.

As we move down below the top of the bubble we still see a strong radial component of velocity, particularly near the gas–liquid interface (see the vector plots on the right side of Fig. 3). Also, the maximum velocity in the developing film is not at the gas–liquid interface but ap-
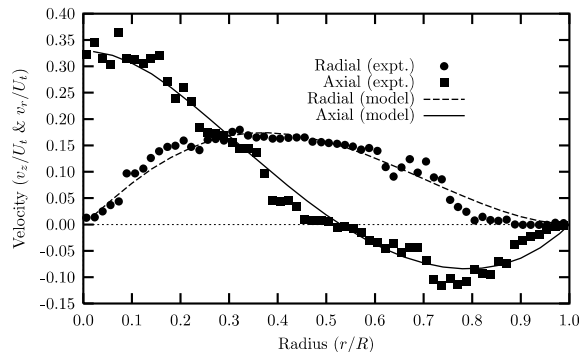

Fig. 5. The axial and radial components of velocity at $z/D = -0.111$ (i.e. just above the bubble). The PIV measurements are compared to the numerical results. This location corresponds to section A in Fig. 3.
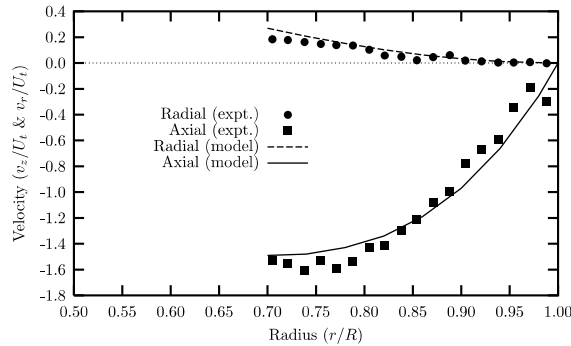
Fig. 6. The axial and radial components of velocity at $z/D = 0.504$. The PIV measurements are compared to the numerical results. This location corresponds to section B in Fig. 3.

proximately half way between the wall and the interface. Moving lower, the radial velocity reduces significantly and the maximum axial velocity moves towards the gas–liquid interface. Fig. 6 compares the measured and predicted velocity fields at the location indicated by B in Fig. 3. Again, the comparison is quite favourable. Although the film is not yet fully developed at this location, the maximum axial velocity has moved very close to the gas–liquid interface.

The film continues to accelerate and thin as it falls until the shear stress at the wall is capable of supporting the weight of the film and a fully developed film is formed. The radial velocity in the film is then zero and the axial velocity profile no longer changes. This axial velocity profile is shown in Fig. 7 along with the theoretical profile developed by Brown (1965) and the numerical predictions. The analysis of Brown (1965) and the numerical model predict a gas–liquid interface location of $r/R = 0.75$ and $r/R = 0.76$, respectively. PIV measurements are not available close to the gas–liquid interface because of excessive laser light reflected off the bubble surface.

Fig. 8 shows the velocity field in the wake of the Taylor bubble. Before discussing the velocity field the shape of the bubble will be considered. As shown in Fig. 8, the bottom of the bubble is
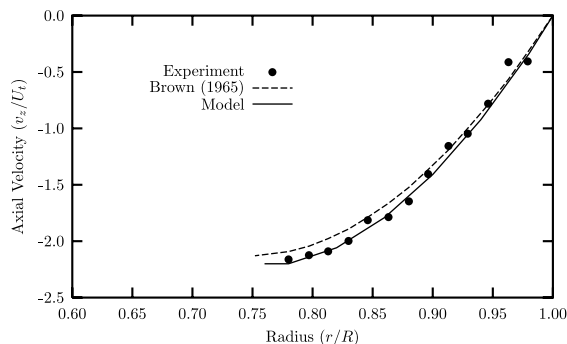

Fig. 7. Velocity profile in the fully developed falling film beside a rising Taylor bubble. The PIV measurements are compared to the analytic solution of Brown (1965) and the numerical results.
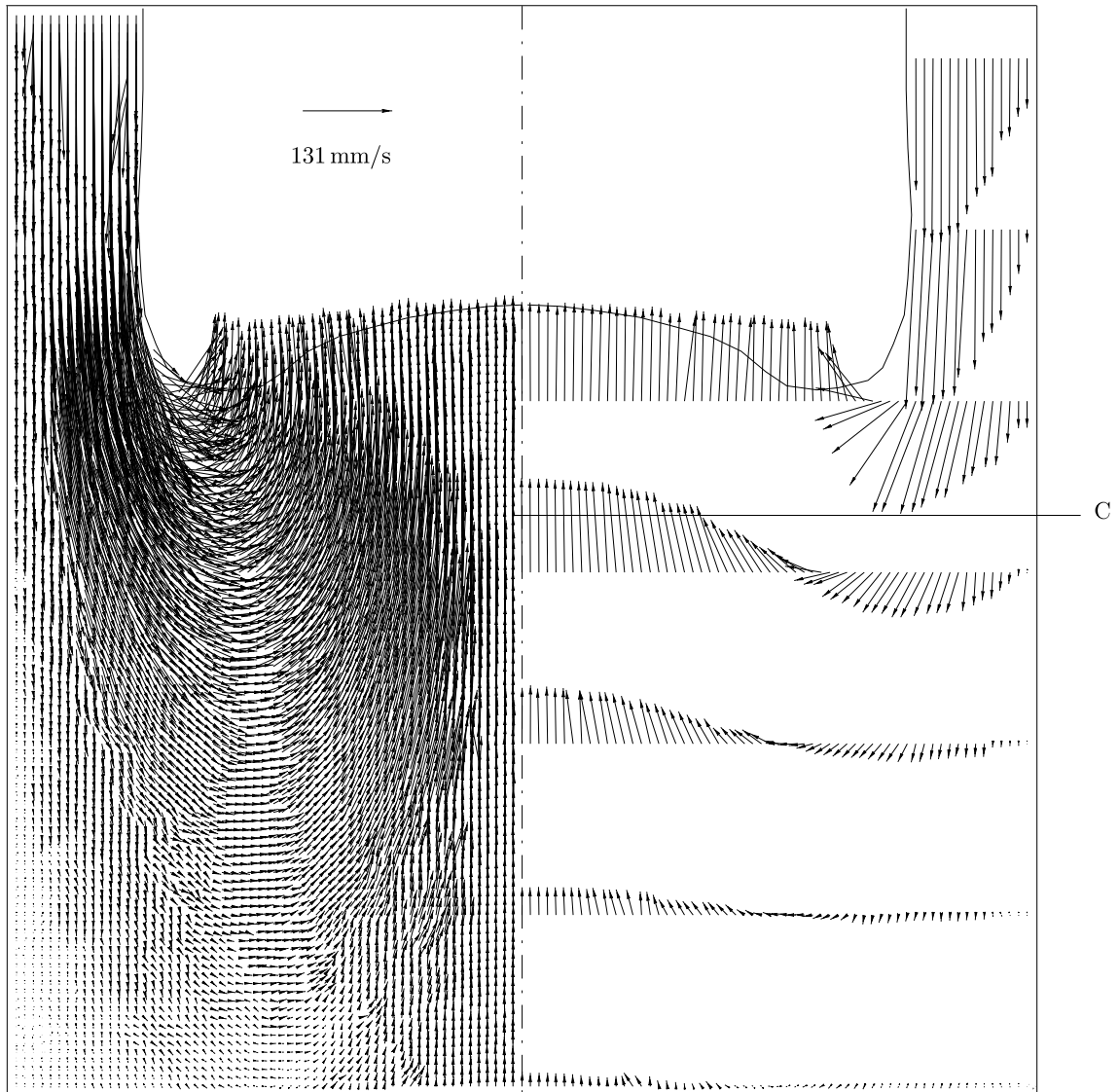
Fig. 8. PIV measurements of the velocity field in the wake of a Taylor bubble rising in a stagnant fluid. The left side of the axis of symmetry shows all the measurements while the right side shows only every twentieth axial location for clarity. The tube diameter is 19 mm.

indented. This profile was sketched by hand directly from the PIV image. The interface position shown is consistent with the results of conventional photographs taken of the bubbles. It is estimated that the interface position can be located to within ± 3 pixels which corresponds to ± 0.06 mm. Because the bubble is axisymmetric, the indented portion is actually obscured by the near-wall portion. However, it is faintly visible in the original image. The prediction of the bubble
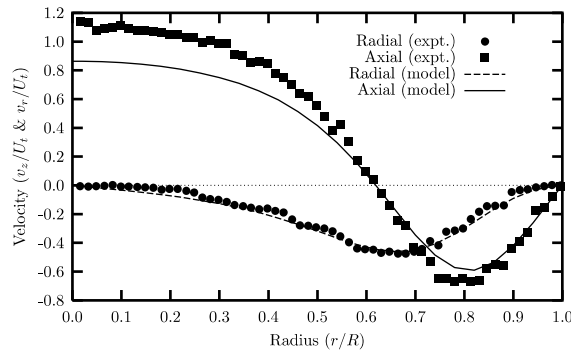
Fig. 9. The radial and axial components of velocity at $z/D = D/5$ (below the Taylor bubble). The PIV measurements are compared to the numerical results.

shape by the numerical model presented in Bugg et al. (1998) is similar to Fig. 8 although some small differences appear to have impacted the prediction of the velocity in the wake. This point will be discussed further shortly.

As was clear at the top of the bubble, a strong radial velocity component exists in the wake region. Here it serves to return the liquid in the falling film to the centreline of the tube. The fluid immediately under the bubble is essentially moving upward at the velocity of the bubble. The axial velocity along the tube centreline falls off with increasing distance from the bottom of the bubble. At the bottom of the field of view, which is about $0.77D$ below the bubble, the axial velocity has reduced to $0.1U_t$.

Fig. 9 compares the axial and radial components of velocity just below the bubble to the numerical predictions. The location of these measurements is indicated by C in Fig. 8. At this location, the high velocity falling film has decelerated to $v_z/U_t = -0.65$ from its maximum of $v_z/U_t = -2.3$ in the equilibrium falling film. An interesting feature of the falling film at the bottom of the bubble is that significant deceleration of the film occurs because of the rounded shape of the bubble bottom near the wall. The numerical predictions are also shown in Fig. 9. The radial component of velocity is very well predicted by the numerical model. However, the axial component is underpredicted in the region of the decelerating falling film. It appears that the falling film is penetrating the fluid below the bubble somewhat more than predicted. The maximum velocity in this region is underpredicted by about 15%. This is likely related to slight differences in the predicted shape of the bottom of the bubble. The bottom edge of the bubble is not as rounded in the predictions as in the experiments and this most certainly effects the way in which the falling film interacts with the fluid below the bubble. Note also that the axial velocity at the tube centreline ($r/R = 0$) is underpredicted. The net mass flow across any plane below the bubble must be zero. Both the numerical and experimental results fulfill this requirement. Due to the axisymmetric nature of the velocity field, a relatively modest underprediction near the wall will correspond to a more dramatic underprediction near the centreline.

A more extensive set of experimental velocity profiles around the Taylor bubble is presented in Fig. 10. This figure shows both axial and radial velocity components for four additional profiles in the nose region and three additional profiles in the wake region. For clarity, smooth curves have
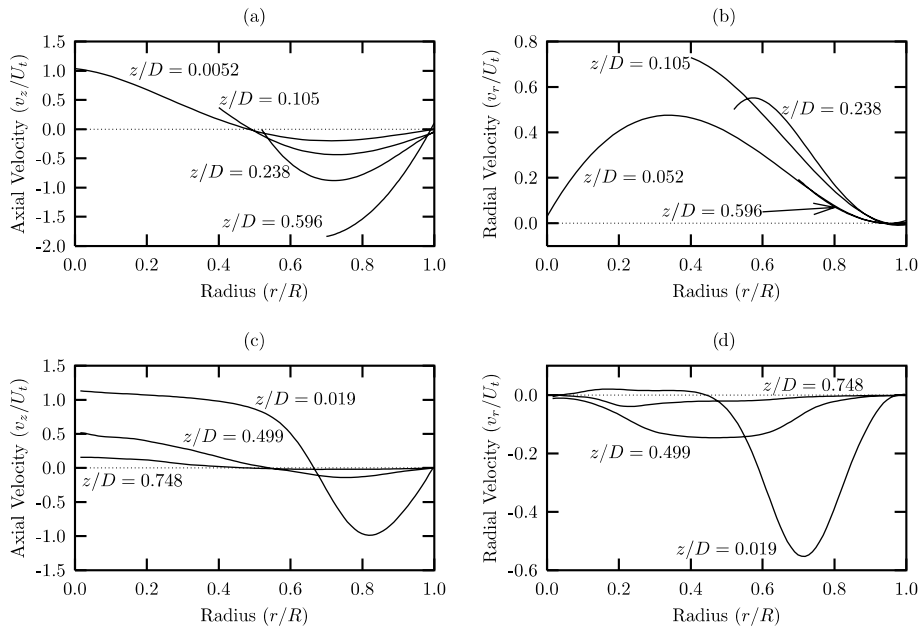
Fig. 10. Summary of PIV measurements around a rising Taylor bubble including (a) the axial velocity near the nose, (b) the radial velocity near the nose, (c) the axial velocity in the wake, (d) and the radial velocity in the wake. Near the nose, z is measured from the tip of the bubble while in the wake z is measured from the bottom of the bubble. For clarity, only smooth curves through the experimental points are shown.

been drawn through the measurements rather than showing the measurements themselves as was done in previous figures. The evolution of the velocity profiles around the bubble shown in this figure are consistent with the earlier discussion.

5. Conclusions

1. Successful, high-resolution PIV measurements were made around a Taylor bubble rising in a stagnant liquid. A spatial resolution of 0.152 mm was achieved in the region above the bubble, in the falling film, and in the wake. The tube diameter was 19 mm.
2. For the conditions tested, the flow is laminar. The velocity profile in the lower portion of the falling film fits the theoretical solution for a viscous falling film very well. Also, the wake region displays the orderly, repeatable characteristics of a laminar flow.
3. The influence of the bubble on the surrounding stagnant liquid is really quite limited. The velocities in the liquid reduce to less than 5% of the bubble speed at $D/3$ ahead of the bubble. The influence of the wake extends further with the velocity dropping to 10% of the bubble speed at about $0.77D$ below the bubble.
4. The numerical model presented in Bugg et al. (1998) predicts these experimental results rather well. The comparison was presented on the basis of detailed velocity field information.

Acknowledgements

References

Brown, R.A.S., 1965. The mechanics of large gas bubbles in tubes I. Bubble velocities in stagnant liquids. Can. J. Chem. Eng. 43, 217–223.

Bugg, J.D., Mack, K., Rezkallah, K.S., 1998. A numerical model of Taylor bubbles rising through stagnant liquids in vertical tubes. Int. J. Multiphase Flow 24, 271–281.

DeJesus, J.D., Ahmad, W., Kawaji, M., 1995. Experimental study of flow structure in vertical slug flow. In: Proceedings of the 2nd International Conference on Multiphase Flow, Kyoto, April 3–7.

Fabre, J., Liné, A., 1992. Modelling of two-phase slug flow. Ann. Rev. Fluid Mech., 21–46.

Hirt, C.W., Nichols, B.D., 1981. Volume of fluid (VOF) method for the dynamics of free boundaries. J. Comp. Phys. 39, 201–225.

Mao, Z.-S., Dukler, A.E., 1990. The motion of Taylor bubbles in vertical tubes I. A numerical simulation for the shape and rise velocity of Taylor bubbles in stagnant and flowing liquids. J. Comp. Phys. 91, 132–160.

Mao, Z.-S., Dukler, A.E., 1991. The motion of Taylor bubbles in vertical tubes II. Experimental data and simulations for laminar and turbulent flow. Chem. Eng. Sci. 46, 2055–2064.

Polonsky, S., Shemer, L., Barnea, D., 1999. The relation between the Taylor bubble motion and the velocity field ahead of it. Int. J. Multiphase Flow 15, 957–975.

Saad, G.A., Bugg, J.D., 2001. PIV measurements around a rising Taylor bubble in a stagnant fluid. In: Proceedings of the 4th International Conference on Multiphase Flow, New Orleans, May 27–June 1.

White, E.R., Beardmore, R.H., 1962. The velocity of rise of single cylindrical air bubbles through liquids contained in vertical tubes. Chem. Eng. Sci. 17, 351–361.